remote sensing

MDPI

Article

Retracking Cryosat-2 Data in SARIn and LRM Modes for Plateau Lakes: A Case Study for Tibetan and Dianchi Lakes

Xiaoli Deng [1,*], Ren-Bin Wang [2], Fukai Peng [3], Yong Yang [2] and Nan-Ming Mo [2]

[1] School of Engineering, The University of Newcastle, New South Wales, NSW 2308, Australia
[2] College of Architecture and Civil Engineering, Kunming University, Kunming 650093, China; kmxywrb@kmu.edu.cn (R.-B.W.); Yong.Yang@kmu.edu.cn (Y.Y.); Nanming.Mo@kmu.edu.cn (N.-M.M.)
[3] School of Geospatial Engineering and Science, Sun Yat-sen University, Zhuhai 519082, China; pengfk@mail.sysu.edu.cn
* Correspondence: xiaoli.deng@newcastle.edu.au

Abstract: This paper estimates lake level variations over two small and adjacent lakes in the Tibetan plateau (TP), namely Gemang Co and Zhangnai Co, as well as the inland Dianchi Lake in China using CryoSat-2 SARIn-mode and LRM 20-Hz waveforms over the period of 2011–2018. Different retrackers and a dedicated data editing procedure have been used to process CryoSat-2 data for determining the lake level time series. The lake level estimations are indirectly validated against those from Jason-2 in TP and from in situ data in Dianchi Lake, both showing good agreement with strong correlation coefficients >0.74. The results of this paper suggest that the official ICE retracker for LRM data and APD-PPT retracker for SARIn-mode waveforms are the most appropriate retrackers over Dianchi Lake and TP lakes, respectively. The trend estimates of the time series derived by both retrackers are 61.0 ± 10.8 mm/yr for Gemang Co and Zhangnai Co in TP, and 30.9 ± 64.9 mm/yr for Dianchi Lake, indicating that the lake levels over three lakes were continuously rising over the study period. The results of this study show that CryoSat-2 SARIn-mode data can be used for monitoring many small lakes that have not been measured by other altimetry missions in TP.

Keywords: CryoSat-2; waveform retracker; Tibetan Plateau; Yunnan Plateau; lake level variation

Citation: Deng, X.; Wang, R.-B.; Peng, F.; Yang, Y.; Mo, N.-M. Retracking Cryosat-2 Data in SARIn and LRM Modes for Plateau Lakes: A Case Study for Tibetan and Dianchi Lakes. *Remote Sens.* **2021**, *13*, 1078. https://doi.org/10.3390/rs13061078

Academic Editors: José Darrozes and Hyongki Lee

Received: 15 January 2021
Accepted: 5 March 2021
Published: 12 March 2021

1. Introduction

There are approximately 1400 lakes in the Tibetan Plateau (TP) [1] and 40 lakes in the Yunnan plateau [2] with water surface area larger than 1.0 km^2. The temporal and spatial variations in water levels of these lakes provide a significant indicator of changes in regional hydrology, ecosystem and climate systems. An improved understanding of lake level variations will thus significantly benefit the adaptive management of these systems. Most lakes in TP have no in situ measurements due to their most inaccessible and remote locations. Since 1992, data from conventional satellite altimetry missions (e.g., TOPEX/Poseidon, Envisat, Jason-1/2/3, SARAL/AltiKa and ICESat) and new generation altimetry missions (e.g., CryoSat-2, Sentinel-3A and ICESat-2) have been used to monitor the temporal lake levels in TP, e.g., [1,3–13].

The altimetry satellite CryoSat-2 was launched on 8 April 2010 with the original focus on monitoring Earth's land and marine ice fields. The most important payload of CryoSat-2 is the SAR (synthetic aperture radar) Interferometric Radar Altimeter (SIRAL), which comprises a conventional pulse-limited radar altimeter, a second antenna, and synthetic aperture and interferometric signal processing system [14,15]. SIRAL operates in three sensor modes depending on the geographical mask for different areas: the low-resolution mode (LRM), SAR mode and SAR interferometric (SARIn) mode. LRM operates like a conventional altimeter in the pulse-limited mode over oceans, land and flat ice sheets; SAR mode mainly works over sea ice and a few ocean areas; and SARIn mode is used around ice sheet margins and over mountain glaciers. SIRAL has different footprint sizes

on ground depending on the sensor mode. When considering the antenna illuminated area, the width of footprint is ~1.65 km for LRM, while this is ~300 m and ~15 km in the along-track and across-track directions, respectively, for both SAR and SARIn modes [14]. CroySat-2 has a long repeat cycle (369 days) with sub-cycles of 30 days and a drifting ground track, producing a spatially dense coverage (~4 km of track spacing at equator) on the Earth surface. This provides a unique opportunity to monitor many small lakes and narrow river systems that were impossible by other altimeters, e.g., [8,16].

One particular challenge in retrieving the water surface height over lakes from altimeters has come from the surrounding topography where reflections from land or vegetation may contaminate the water signal. When SIRAL is operating in LRM near the lake bank, the topography effects first appear on the waveform trailing edge and then move towards the leading edge. Over the TP area, SIRAL is operating in SARIn mode. A feature of SARIn mode is that SIRAL can directly detect off-nadir measurements that are located within its rectangular footprint (i.e., 0.3 × 15 km). The waveform obtained near the lake bank may contain signals reflected from land and water surfaces, showing distinguishable peaks. Therefore, it is vital to develop dedicated retracking algorithms for CryoSat-2 waveforms, so that the altimeter range between satellite and nadir water surface can be correctly estimated.

In the past years, many dedicated retrackers have been developed for CryoSat-2 LRM and SARIn-mode waveforms to retrieve water levels over lakes and rivers, e.g., [16–20]. These retracks can be classified as physical-based and empirical algorithms. One of physical-based retrackers was developed by [19]. The retracking method assumes that the peaky waveform corresponds to heights of lake and surrounding terrain surfaces. In order to determine the positions of waveform peaks, the Cryosat-2 SARIn-mode generic waveform is simulated and the cross correlation between simulated and observed waveforms is computed. The heights are computed based on the peak positions. The lake water levels can be determined after the heights caused by surrounding land topography are removed. This is achieved by applying a tailored outlier detection to the along-track height profile. This retracker has been used to determine the water levels and trends of 46 lakes (>110 km^2 per lake) on the TP [3].

Empirical retrackers, such as the offset center of gravity (OCOG) method [21] and threshold method [22], are generally used to retrieve the altimeter range correction for LRM, SAR and SARIn mode waveforms over ice sheets and inland waters. To avoid the effect of waveform peaks caused by signals reflected from land, vegetation or bright target, the primary peak threshold retracker has been applied to sub-waveforms, e.g., [11,17,18,20]. The primary peak is considered as the first peak at the end of leading edge of the waveform, which corresponds to signals returned from the water surface at nadir. The retracker forms the sub-waveform around the primary peak, and then uses the OCOG or threshold method to estimate the retracking correction. The retracker has been found to provide the most reliable results over inland water bodies. For example, the primary peak threshold retracker was applied to CryoSat-2 SARIn-mode waveforms in a study that measures water levels in 50 large lakes (> 150 km^2 per lake) in TP [11].

Most studies using altimetry data focused mainly on the relatively large lake (>110 km^2), as the small lake or water body (<60 km^2) could not be sampled by most satellite radar altimeters. From 2010 onward, CryoSat-2 data are available with high spatial resolution that allows to explore many lakes that cannot be mapped using other altimeters. A recent study [8] estimates water level variations in 61 TP lakes using altimeter data (2003–2017) from CryoSat-2, SARAL and ICESat missions. The officially retracked data provided in Level-2 geophysical data record (GDR) products were directly used. The results show that about two-thirds of lake levels rose in the period of 2010–2016, with the largest rise in the lakes located in northern part of TP. Some of these small lakes, each with the area >27 km^2, included in the results in [8], are interesting enough to motivates a further exploration of the capability of CryoSat-2 data for plateau lakes.

This paper, therefore, aims to test the capability of CryoSat-2 data for monitoring water levels of plateau lakes by conducting a case study for two small lakes (<52 km^2 per lake) using SARIn-mode data in Tibet and an inland lake using LRM data in Yunnan, China. The paper is organized as follows: the study area and data are described in Section 2; the methods used to derive lake levels are presented in Section 3; the results are analyzed and discussed in Section 4; and conclusions are given in Section 5.

2. Study Areas and Data

2.1. Dianchi Lake and Tibetan Lakes

We select Dianchi Lake (Figure 1) and two Tibetan lakes (Gemang Co and Zhangnai Co, Figure 2) in China as a case study on monitoring water level variations of plateau lakes using data from CryoSta-2. These lakes were chosen for three reasons. First, there were no (or a little) altimetry data available over the lakes before the CryoSat-2 mission, such as Gemang Co and Dianchi Lake. Second, these lakes with different surface extensions are representatives for diverse plateau lakes in how lakes will respond to climate and other hydrological changes. Finally, many lakes in TP with similar size (<52 km^2 per lake) to Gemang Co and Zhangnai Co have never been investigated using either in situ data or altimeter data. However, it is essential to monitor these small size lakes, as they altogether make the major contribution to regional hydrology and ecosystems.

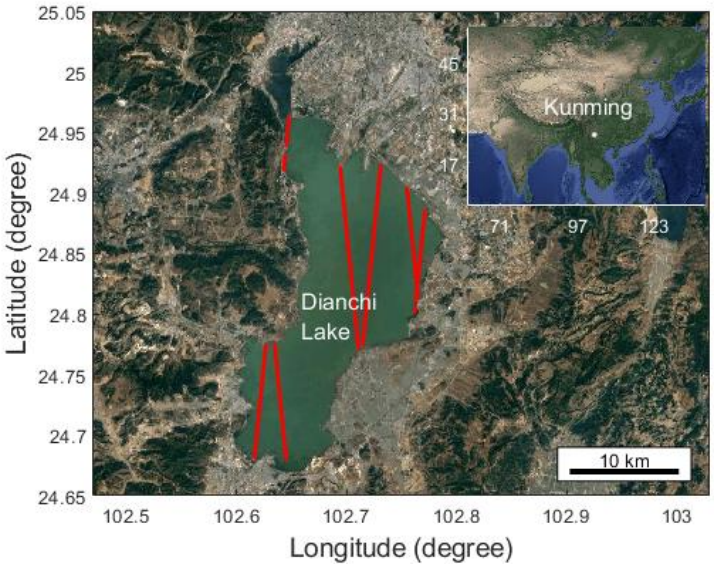

Figure 1. Dianchi Lake, China, overlapped with one cycle of CryoSta-2 LRM ground tracks (in red) in 2011.

Dianchi Lake (102°36′-102°48′ E, 24°39′-25°01′ N) with a surface area of 310 km^2 is located on the southwestern outskirts of the metropolitan city Kunming in Yunnan in the southwest of China. It is the largest faulted freshwater lake in Yunnan plateau [23,24]. It extends 39 km from north to south and 12.5 km from east to west [24]. Its water supply is now mainly relied on precipitation and water transfer projects through the river channels from Niulan River and other out basin lakes [25,26]. The lake provides important water resources for the city due to its geographic location, supporting intensive and modern socio-economic activities around the city. Water level variations are found to be influenced by the periodic signals of 1, 5 and 15 years from a study using in situ gauge data (1961–2016) in [26]. Previous studies have shown that water level variations can generate more productive and diverse habitats, as well as undesirable effects on lake ecosystems and promotion of eutrophication blooms [27].

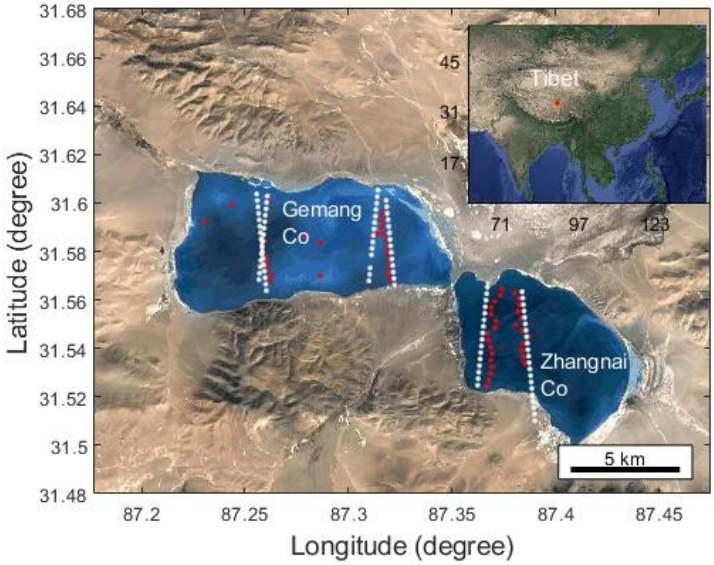

Figure 2. TP lakes Gemang Co (left) and Zhangnai Co (right) overlapped with one cycle of CryoSat-2 SARIn-mode ground tracks in 2016. The white-dot lines are the nominal ground tracks, while the red dots are the corresponding slope-corrected ground tracks when considering off-nadir measurements. Note that some off-nadir measurements are located on land, but have been deleted during the data editing process.

Lakes of Gemang Co (52 km^2, 31.58° N and 87.28° E) and Zhangnai Co (36 km^2, 31.55° N and 87.39° E) are located in south of central TP. They joined as the same lake during the Quaternary Period and separated into two lakes due to the drop of the lake level. Two lakes are linked through a small river. The average annual temperature in the lake is 0 °C, and the average annual precipitation is about 200 mm [28]. Gemang Co had not been sampled by any radar altimetry missions before CryoSat-2, while Zhangnai Co was covered by track 079 of TOPEX/Poseidon and Jason series. During every repeat cycle (i.e., 369 days), Gemang Co and Zhangnai Co are visited four and two times by CryoSat-2, respectively (Figure 2). These tracks allow us to estimate the trend and periodic variations of lake levels over the period of eight years in this study.

The ground track of CryoSat-2 has a near north–south orientation because of its nearly polar orbit. As mentioned in Section 1, CryoSat-2 has a rectangular footprint for SARIn mode and a disk footprint for LRM. This feature causes the polluted waveforms when SARIn-mode trackers pass close to the eastern or western lake shoreline in TP plateau, and when LRM tracks move close to the shoreline of the lake. These polluted waveforms need to be processed by the dedicated retracker and may sometimes not be used to retrieve the reliable lake level. Therefore, a well-designed data editing procedure is necessary, which will be described in Section 3.

2.2. CryoSat-2 LRM and SARIn Mode 20 Hz Data

Eight years (2011–2018) of CryoSat-2 LRM and SARIn mode data (20 Hz) from Baseline-C Level-2 (L2) and Level-1B (L1B) data products were used in this study. Both levels of data products are obtained from European Space Agency (ESA) ftp site: ftp://science-pds.cryosat.esa.int (accessed on 11 March 2021). The Baseline-C L1B data contain the full radar echo waveforms. The range window covers 128 and 1024 data samples for LRM and SARIn mode, respectively. The L1B SARIn-mode waveforms were used over lakes of Gemang Co and Zhangnai Co in TP, while L1B LRM waveforms were used over Dianchi Lake. The L2 data contain the geophysical corrections and surface height estimates.

As shown in Figure 2, CryoSat-2 can measure the off-nadir surface when operating in SARIn mode. For measurements of SARIn mode, the L2 ground location includes any across-track offset, which may be different from that provided in L1B (cf. Figure 2). The

off-nadir measurements need to be carefully handled as they are not measured over the surface at nadir and sometimes on land. Although the off-nadir data can be theoretically corrected by applying the angle of arrival [29], we found that large uncertainty occurs when the off-nadir point is distant from the corresponding nominal nadir point along a ground track. After a series of empirical tests, we filtered out the off-nadir point that has a distance >1.5 km to the nominal nadir point. The distance of 1.5 km might be increased for large and open water bodies, but it is an appropriate criterion for small lakes chosen in this study. In the case of Gemang Co (Figure 2) after applied this criterion, there are only two tracks in most of repeat cycles that provide quality lake level measurements.

2.3. Validation Datasets

It is a challenging task to validate the lake levels estimated from CryoSat-2 against the in situ lake gauge data. There are lake gauges around Dianchi Lake, but the in situ records are unavailable to authors. The validation here is to compare the annually water level variations from CryoSat-2 with those derived from lake gauge records in [25]. Lake level changes from Jason-2 data between 2009 and 2015 in Zhangnai Co were estimated and analyzed by Hwang et al. [13], which were used to assess our results from CryoSat-2. There are no in situ and other altimeter data over Gemang Co, and therefore the validation cannot be conducted.

3. Methods

This section describes the methods that used to retrack CryoSta-2 waveforms (both LRM and SARIn mode) and to generate the lake water levels.

3.1. Retracking Methods

In CryoSta-2 data products, waveforms are processed by different official retrackers to estimate the range from the altimeter to water surface. The official LRM range has two solutions from (1) fitting the Hayne [30] model to waveforms using the maximum likelihood estimator 4-parameter (MLE4) algorithm, and (2) using the ICE OCOG retracking process. The SARIn-mode range is derived by using the Wingham and Wallis [31] model-fit waveform (WWMFW) retracking algorithm [14]. The official ranges derived from ICE and WWMFW retrackers were directly used in this study.

In order to retrieve reliable lake levels, we also retrack waveforms using other retrackers. For SARIn mode waveforms over TP lakes, the OCOG [21] and primary peak threshold (PPT) retrackers [17] are used. The OCOG and PPT retrackers are applied to full- and sub-waveforms, respectively. In addition to the use of PPT retracker, we also truncate the full waveform into a sub-waveform based on the peak detected by the adaptive peak detection (APD) approach by Peng and Deng [32,33]. The APD was originally developed to detect peaks of the LRM waveform, which has been applied to waveforms from Jason-1/2/3 missions. It determines peaks through searching the feature gates of the peak, start and stop, leftfoot and rightfoot points on a waveform, providing the maximum waveform power and width of each peak. The detailed description of the APD can be found in [33]. Since the shape of the SARIn-mode waveform differs from that of the LRM waveform, the original APD has been modified by testing and adjusting its parameters in this study. The sub-waveform is formed based on the APD-detected primary peak, and retracked by the PPT method. This approach is hereafter called as the APD-PPT retracker.

For LRM waveforms over Dianchi Lake, two retrackers used are (1) the modified Brown-peaky (MBP) retracker developed by Peng and Deng [33] and (2) adaptive leading edge subwaveform (ALES) retracker by Passaro et al. [34]. The MBP retracker adopts the Brown [35] model with the second-order Bessel function, which can deal with large off-nadir angles up to 0.8°. Waveform peaks are detected using the APD method. The MBP fits the Brown model to the full waveforms using a weighted least squares estimator, in which the portion of detected waveform peaks is assigned to a small weight (e.g., 0.01) and other part of waveform is assigned to an equal weight (e.g., 1.0). The ALES retracker truncates the

waveform based on a linear relationship between the width of truncated subwaveform and value of significant wave height. It fits the Brown model to the subwaveform to estimate the range correction. Both MBP and ALES have been successfully used to retrack LRM waveforms in different coastal zones around the world [33,34,36,37]. Since Dianchi Lake is a relatively large water body that has more fetch for the wind waves, the LRM waveforms are less likely to be specular than to be contaminated by land when the ground track closes to the lake shoreline. Therefore, MBP and ALES may be capable of retrack the waveforms over the lake.

3.2. Lake Surface Height

The lake surface height, H, with respect to the geoid can be computed as:

$$H = Alt - R - N, \tag{1}$$

where, Alt is the satellite altitude, N the geoidal height at the location, which is interpolated using the Earth gravitational model 2008 (EGM2008) with respect to the WGS84 ellipsoid [38], and R the range between altimeter and water surface, which can be computed as [14],

$$R = \frac{1}{2} c \cdot R_{wd} + C_r + C_g, \tag{2}$$

where, c is the speed of light in vacuum, R_{wd} the window delay of CryoSat-2 measured from the signal emission time to the center of the range window, C_r the retracking range correction computed by retracking waveforms, and C_g the geophysical corrections. The geophysical corrections used in this study include the dry and wet troposphere, global ionospheric maps (GIM) ionosphere, ocean loading tide, solid Earth tide and geocentric polar tide corrections.

3.3. Estimations of the Lake Level and Trend

When processing altimeter waveforms over inland water bodies, it is essential to correctly identify that data are reflected from the water surface but not from surrounding land topography. In this paper, this is achieved by using water masks to exclude altimeter data over land. The water mask for two TP lakes was obtained from the global lakes and wetlands database (GLWD): https://www.worldwildlife.org/pages/global-lakes-and-wetlands-database (accessed on 12 March 2021). The water mask used for Dianchi Lake was derived using the multispectral satellite Sentinel-2 imagery. It can be seen from Figures 1 and 2, these water masks well capture the measurements over lakes.

After waveforms are extracted using the water mask, they are retracked to estimate the retracking range correction, C_r (cf. Equation (2)), using the retrackers as described in Section 3.1. The 20 Hz along-track surface heights with respect to EGM2008 are then computed using Equation (1) over the lake. The median value of retracked along-track heights are taken as the lake level. Using a specifically designed data editing procedure, we remove outliers and surface heights corresponding to land topography for estimating the optimal lake levels and trend following the steps below.

1. Outliers in along-track retracked surface heights are detected and removed track by track using the generalized extreme studentized deviate (ESD) test [39]. The generalized ESD test is capable of detecting one or more outliers in a univariate dataset, which has been widely used in data analysis. We also tried to remove outliers using a 3-sigma filter (equivalent to a 99.75% confidence level), but found that the generalized ESD test has high sensitivity in detecting outliers in our cases.
2. The bias between retracked surface heights from different retrackers due to using different retracking algorithms are removed. Here, we simply calculate the bias as the mean of differences between along-track retracked heights from different retrackers due to the relatively small size of lakes. The method has been used to calculate sea-surface-height bias over oceans, e.g., [40].

3. The median value and standard deviation are computed from the outlier-free and unbiased surface heights along each track. This is to form the time series of the lake levels and the quality estimation from CryoSat-2 measurements over the lake.
4. The trend of lake level variations are estimated by fitting a harmonic function to the time series.

The above data editing procedure does not consider the water surface slope correction caused by the low-resolution geoid and/or wind induced effects, which was made due to the size and orientation of lakes. The slope correction is necessary, in particular for lakes with the large west to east extent [9]. This is because CryoSat-2 passes over different parts of the lake in each cycle, and the geoid variation or wind induced effects can thus introduce errors when computing the lake level using surface heights from different tracks [3,8,9]. In this study, however, the west to east extent of the lakes is relatively small. The maximum difference between geoidal heights on the west and east coasts of lakes is less than 0.1 m, and therefore the slope correction can be safely neglected.

4. Results and Discussions

4.1. Results of Gemang Co and Zhangnai Co

This section presents the lake levels derived from CryoSat-2 SARIn-mode waveforms over Gemang Co and Zhangnai Co in TP. The comparison with available resources will also be discussed.

4.1.1. SARIn-Mode Waveforms

During retracking processing, we analyzed the waveform features over selected TP lakes. Figure 3 shows two examples of along-track SARIn-mode waveforms and sigma-0 on 16 June 2016 and 3 December 2016. The peaky waveforms can be clearly seen in Figure 3a with the highest power shown on the first peak when the track passes through lake Gemang Co. Although these waveforms have a narrow width in common, specular waveforms appeared over Zhangnai Co on 3 December 2016 (Figure 3b). The radar backscattering coefficient, sigma-0, has been used as an indicator when classifying reflected surface features. A sigma-0 value >10 dB, for instance, was used in [10] as one of threshold levels to select waveforms returned from lake water surfaces. In our study from Figure 3c,d, it is observed that the values of sigma-0 in December are much larger (28–38 dB) than those (6–14 dB) in June, suggesting that lakes have seasonal surface characteristics.

Many TP lakes freeze up in winter between November and February, when lakes experience the annual maximum wind speed and minimum temperature. The ice gradually breaks up with an increase in temperature of the air (water) above (below) the ice in spring. For lakes around latitude 31.0° N, a study by [41] found that the annual duration of completed and incomplete ice cover is in average 72 days and 126 days, respectively, using the MODIS 8-day composite data over a period from 2001 to 2010. Since both selected lakes in this paper are located around the latitude 31.6° N, they fall into the category of TP lakes in [41]. The annual ice-cover cycle of freeze-up and break-up leads to an abrupt change of lake surface properties, affecting values of sigma-0 and shapes of waveforms over lakes. This explains the cause for the appearance of specular waveforms and large values of sigma-0 in winter months over TP lakes.

As illustrated in the above results, the precise water mask is essential when retracking SARIn-mode waveforms to retrieve the surface heights close to the lake shoreline over TP lakes. This can be achieved with the supplement of satellite imagery data from Landsat or Sentinel-2, such as what we did for Dianchi Lake in this study, which is our ongoing project.

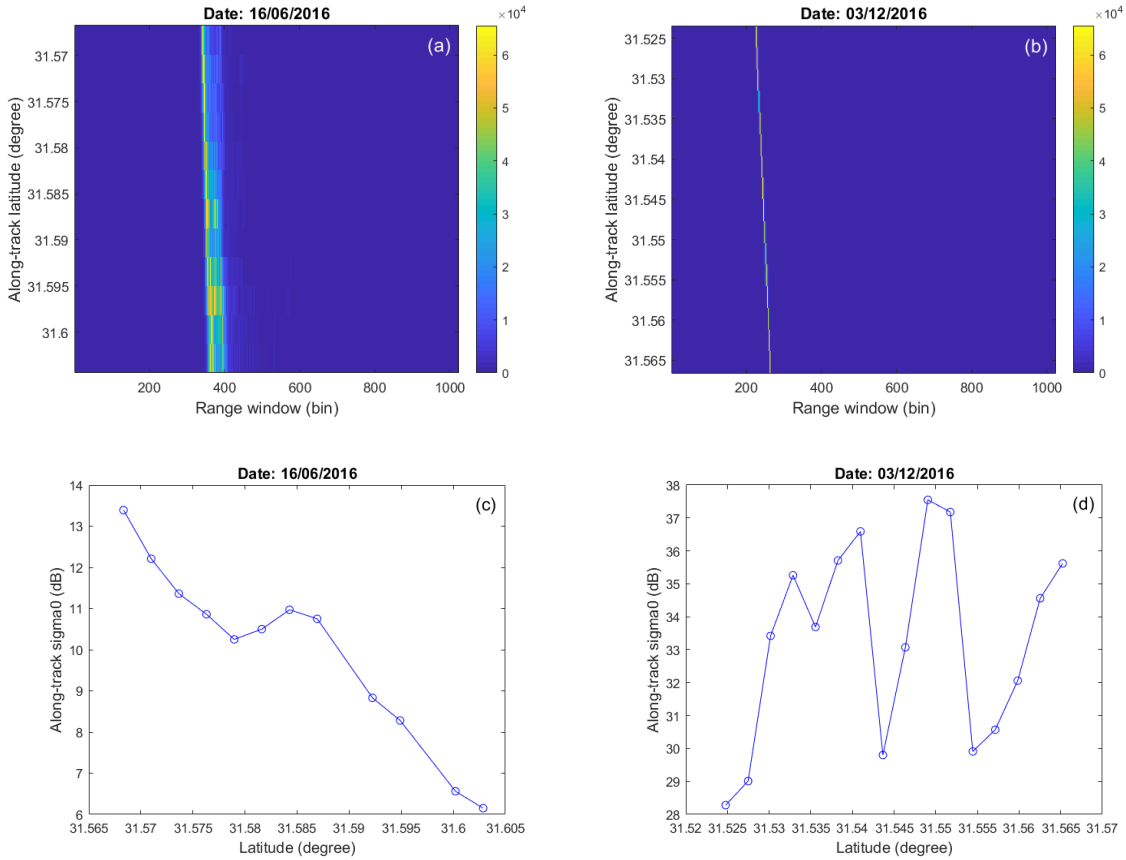

Figure 3. CryoSat-2 along-track SARIn-mode waveforms and sigma-0 over lakes of Gemang Co (**a**,**c**) and Zhangnai Co (**b**,**d**). The color bar in (**a**,**b**) presents the power of waveforms.

For some tracks it was not possible to retrieve lake surface heights because of a high level of disruption in the SARIn-mode measurements. This was most likely to be attributed to the effect of SARIn-mode off-nadir measurements outside (or inside) of the lake. We again excluded the off-nadir point that has a distance >1.5 km to the nominal nadir point as discussed in Section 2.2.

4.1.2. Surface Height Profiles over Gemang Co and Zhangnai Co

Waveforms along the selected tracks over two lakes were retracked using different retrackers described in Section 3.1: WWMFW, PPT, OCOG and APD-PPT. The data editing procedure described in Section 3.3 was then applied to remove outliers and derive the surface heights with respect to the EGM2008 geoid. Over both lakes, the along-track measurements are taken less than one second due to their small sizes. The geoid gradient correction is not considered as the size of lakes is <52 km^2. Figures 4 and 5 show the along-track surface height profiles corresponding to waveforms in Figure 3a,b, respectively. It can be seen that the along-track surface height profiles from different retrackers have in general a similar variation pattern. However, it can be seen that the official WWMFW retracker has larger fluctuating surface heights than other retrackers.

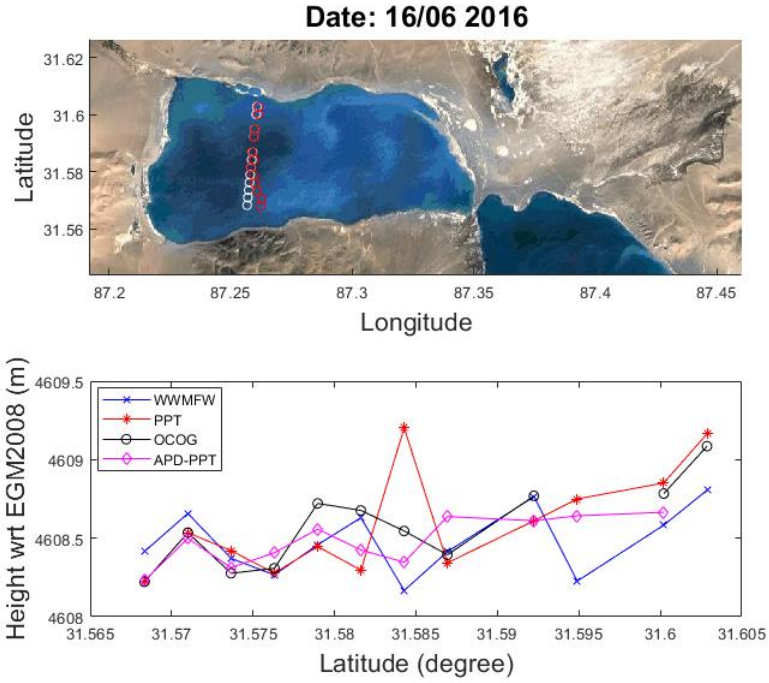

Figure 4. The CryoSat-2 track (top) and its retracked surface height profile (bottom) on 16 June 2016 over lake Gemang Co, which corresponds to the peaky waveforms shown in Figure 3a and were retracked by retrackers of the Wingham and Wallis model-fit waveform (WWMFW) algorithm, primary peak threshold (PPT), OCOG and our APD-detected primary peak threshold (APD-PPT). Outliers and bias have been removed using the method described in Section 3.3.

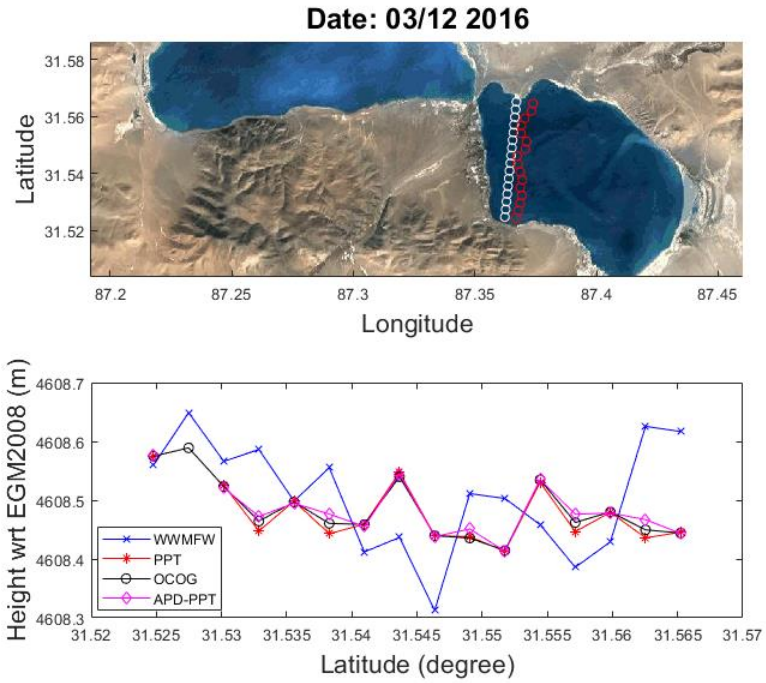

Figure 5. Similar to Figure 4 but over lake Zhangnai Co and corresponding to the specular waveforms shown in Figure 3b on 3 December 2016.

In order to determine the lake level variations, the median value of surface heights and standard deviation were computed along each track. The lake level variations derived from four retrackers over the period of 2011–2018 are presented in Figure 6, while the statistics of standard deviations are listed in Tables 1 and 2.

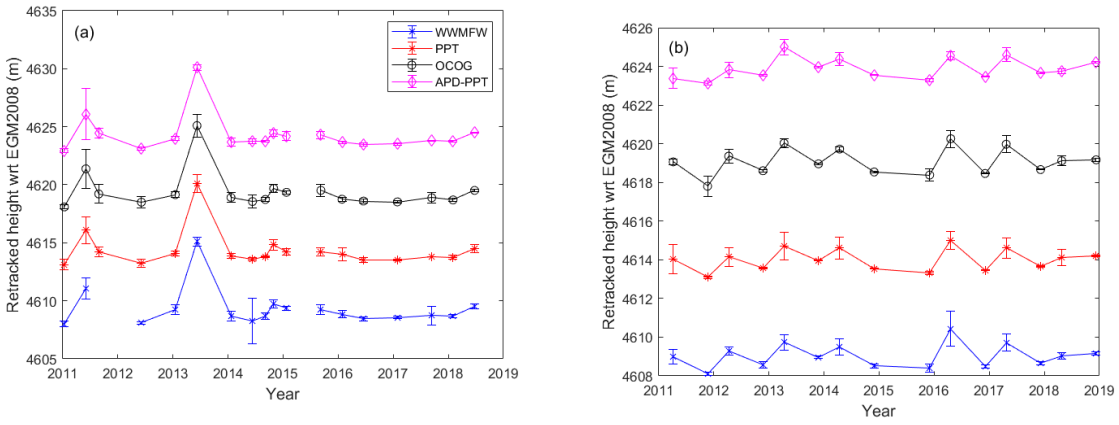

Figure 6. Lake level variations with error bars for (**a**) Gemang Co and (**b**) Zhangnai Co. Both (**a**,**b**) share the same labels shown in (**a**). Arbitrary constants (5 m) are added for visual clarity of lake levels of each retracker.

Table 1. Statistics of maximum, minimum and mean standard deviations of the lake level, generated from along-track water surface heights, for lake Zhangnai Co. The rightmost column lists the number of lake levels measured between 2011 and 2018. The bold value indicates the smallest mean standard deviation.

Retracker	Max (m)	Min (m)	Mean (m)	No
WWMFW	1.956	0.079	0.433	17
PPT	1.155	0.014	0.344	18
OCOG	1.688	0.080	0.424	18
APD-PPT	2.200	0.029	0.303	18

Table 2. As for Table 1 but for lake Gemang Co.

Retracker	Max (m)	Min (m)	Mean (m)	No
WWMFW	0.901	0.070	0.253	15
PPT	0.746	0.022	0.284	15
OCOG	0.535	0.022	0.204	15
APD-PPT	0.540	0.023	0.186	15

It is noted that there are four tracks in one repeat cycle passing through Gemang Co (cf. Figure 2). After removing the outliers by applying the data editing procedure, however, there are usually two tracks in most of cycles that can be used to derive the reliable lake levels over Gemang Co (Figure 6a). Tracks around September and October are excluded in most years, with the exception in 2014 when all four tracks were used. The reason for the poor quality tracks is not clear, but one can speculate that SARIn-mode off-nadir waveforms are seriously contaminated by surrounding land. It is found that the elevation of surrounding mountains, except for the eastern side of the lake, is at least about 100–200 m higher than the lake level over Gemang Co, causing a large number of off-nadir measurements on mountains. Therefore, some tracks may not provide reliable measurements. Two tracks passing Zhangnai Co are not affected and can be used over the entire study period (Figure 6b).

It can be seen from Figure 6 that the time series of lake levels from four retrackers show again a similar variation pattern over each lake. For Gemang Co, the lake level could not be derived by all retrackers in June 2015. This was found through a screening check that all along-track waveforms were found to be poor quality. The official WWMFW retracker failed to estimate the lake level in August 2011, when other retrackers retrieved the reasonable lake level with good agreement. The lake levels increase up to ~4–5 m in June 2011 and 2013, but show a relatively smooth variation after 2013 (Figure 6a). For Zhangnai

Co, the lake levels present an obvious annual cycle, which is low around December and high around April (Figure 6b). There was a strong El Niño event recorded between 2015 and 2016, when a dramatic decrease in precipitation occurred in TP [42]. The anomalous lake level variations have been found in some lakes in central TP by Lei et al. [42]. In this study, however, the lake level variations in both lakes seem not to be clearly affected by the 2015–2016 El Niño event, and are still continuing their long term change patterns. The trend of lake levels derived from the 8-year CryoStat-2 SARIn-mode data can be estimated for both lakes, through the length of time series may not be long enough for a robust trend estimation. The trend estimates are shown in the next section.

From Tables 1 and 2, our APD-PPT retracker has the best performance and achieves the smallest mean standard deviations of the lake levels, with 0.303 m for Gemang Co and 0.186 m for Zhangnai Co, when compared to other retrackers.

4.1.3. Validation

There is no in situ data available to the authors that can be used to evaluate the retracked lake levels, in particular to assess our approach that is applied in this study. Here, we made an indirect validation for Zhangnai Co by comparing the lake levels derived from CryoSat-2 SARIn-mode 20 Hz data (2011–2018) in this study with those derived by Hwang et al. [13] using one track of Jason-2 LRM 20 Hz data (2009–2015). Two sets of time series have an overlap between 2011 and 2015. However, they are relevant to different satellite orbits, and there is the bias between lake levels derived from CryoSat-2 and Jason-2 measurements due to the use of different retracking algorithms and data editing methods. These make it impossible to direct compare the two data sets. Therefore, we first transferred Jason-2 data from the TOPEX ellipsoid to the WGS84 ellipsoid, and then computed the lake level anomalies.

The comparison was conducted using the lake level anomalies (Figure 7). It can be obviously seen that the peaks of lake fluctuations of Jason-2 (up to ~15 m) are different to those of CryoSat-2 (up to ~3 m). The main reason for this may be due to the revisit time of the satellite. Jason-2 repeats its orbit every 10 days, revisiting the same track about 36 times per year over Zhangnai Co. CryoSat-2 has a 369-day repeat orbit and collects measurements from two tracks around April and December every year. Thus, Jason-2 has a higher temporal resolution than CryoSat-2 for observing lake level variations.

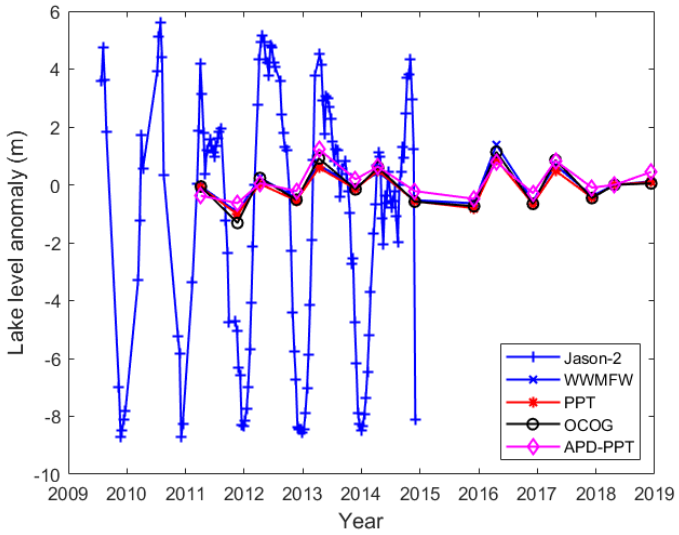

Figure 7. Validation of lake level variations derived from CryoSat-2 against those from Jason-2 over Zhangnai Co. The lake level anomaly is computed by subtracting a median value of lake levels between 2011 and 2015 from each lake level.

It also can be seen that the lake levels from Jason-2 and CryoSat-2 exhibit a similar trend. By fitting a harmonic function to the retrieved lake level, the linear trends can be estimated using 7-year Jason-2 (2009–2015) and 8-year CryoSat-2 (2011–2018) time series of lake level anomalies. The trend estimation over a similar time span will provide a measure for comparison of two different lake level time series. The correlation coefficients between retracked CryoSat-2 and Jason-2 data sets over the period of 2011–2015 are computed. The median absolute deviation of CryoSat-2 lake levels with respect to Jason-2 (2011–2015) is also computed, with the smallest value indicating the lowest noise level (or uncertainty) of retracked data. The estimations of trend, median absolute deviation and correlation coefficient are listed in Table 3. For CryoSat-2 the trends in relation to different retrackers range from 51.1 to 61.0 mm/yr during 2011–2018, while for Jason-2 the trend is 59.9 mm/yr during 2009–2015. The trend estimates from CryoSat-2 time series agree well with that from Jason-2 data sets. The correlation coefficients (>0.7) indicate a strong correlation between lake level anomaly estimates derived from Jason-2 and CryoSat-2 measurements over the period of 2011–2015. The median absolute deviations range from 0.234 to 0.434 m with the minimum value for APD-PPT retracked lake levels, indicating again that APD-PPT is the most appropriate retracker for CryoSat-2 SARIn-mode waveforms over Zhangnai Co.

Table 3. Estimates of trends, correlation coefficients and median absolute deviation (MAD) of CryoSat-2 (C2) SARIn-mode and Jason-2 (J2) LRM measurements over Zhangnai Co.

Mission	Retracker	Trend (mm/yr)	Period	Correlation [1]	MAD (m)	Period [3]
C2	WWMFW	55.3 ± 10.8	2011–2018	0.76	0.434	2011–2015
C2	PPT	51.1 ± 10.8	2011–2018	0.73	0.323	2011–2015
C2	OCOG	61.5 ± 10.8	2011–2018	0.73	0.322	2011–2015
C2	APD-PPT	61.0 ± 10.8	2011–2018	0.74	0.234	2011–2015
J2	[13] [2]	59.9 ± 5.8	2009–2015			

[1] Correlation between CryoSat-2 and Jason-2 lake level anomalies. [2] Jason-2 lake levels are adopted from those retracked by Hwang et al. [13]. [3] This is the period for computations of the correlation and MAD.

The validation results suggest that APD-PPT can efficiently retrieve linear lake level variations from CryoSat-2 SARIn-mode 20 Hz data for relatively small lakes (<52 km^2) in TP plateau. This is important as most TP small lakes, which have never been sampled by other altimetry satellites, can now be monitored by APD-PPT retracked lake level time series.

The trends related to time series of lake levels from different retrackers were also estimated for Gemang Co. These are 76.9, 59.6, 51.3 and 61.0 mm/yr with respect to retrackers of WWMFW, PPT, OCOG and APD-PPT, respectively. Since there are neither the in situ data nor other altimeter measurements over Gemang Co, the validation of lake levels cannot be conducted. However, the same approach applied to Zhangnai Co was used for Gemang Co, and hence it can be inferred from the above validation results that the quality of lake levels over Gemang Co is similar to that of Zhangnai Co. The rising trends over both Gemang Co and Zhangnai Co are consistent with those of surrounding lakes in [8], where the trends of nearby lakes are 80 mm/yr for Dagze Co and 120 mm/yr for Ngangzi Co from CryoSat-2 SARIn-mode data between 2010 and 2016.

4.2. Results of Dianchi Lake

This section presents the lake levels derived from CryoSat-2 LRM 20 Hz waveforms over Dianchi Lake. The validation against available data resources will also be discussed.

4.2.1. LRM Waveforms

Dianchi Lake has a south to north extent and irregular shape though it has a relative large area of 310 km^2 (Figure 1). CryoSat-2 operates in the LRM over Dianchi Lake, and

thus measurements are taken within an altimeter footprint width of 1.65 km. Along-track waveforms close to the lake shoreline can again be polluted by land, in particular near the north-western and eastern sizes of the lake where the tracks are parallel to the lake shoreline (cf. Figure 1). Figure 8 shows an example of along-track waveforms when the same track passing the lake in different revisit time (Figure 8a). Track in white is closer to the shoreline in the eastern side than the track in red. The waveforms along white and red tracks are shown in Figure 8b,c, respectively. It can be seen that almost all waveforms along the white track have exhibited the land waveform feature (Figure 8b), which has no clear leading edge due to the effect of land returns. When the track (in red) moves further away from the shoreline, the along-track waveforms become typical LRM water waveforms with obvious leading edge except for a few points at the two ends of track (Figure 8c). In the case of these two tracks, the white track was not used to retrieve lake surface heights. In order to estimate reliable lake levels, we only used the measurements that have a distance >2 km to the shoreline in this study and took into account of the LRM's footprint size and CryoSat-2's north–south orbital orientation.

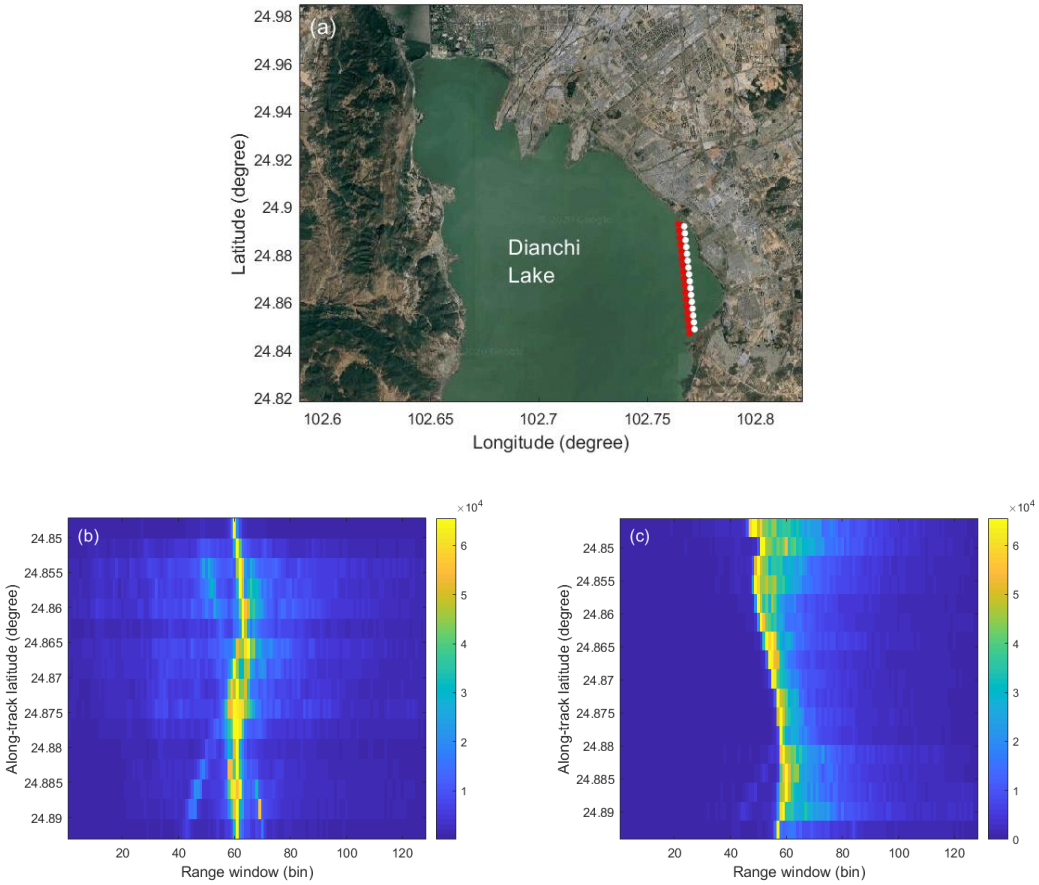

Figure 8. (**a**) A Cryostat-2 track passing Dianchi Lake at different time; (**b**,**c**) LRM waveforms along white and red tracks in (**a**), respectively.

4.2.2. Lake Surface Heights

For CryoSat-2 LRM operation, the retracked lake level was estimated by a median value of retracked surface heights along a track. After applying the data editing procedure, the surface heights were obtained from tracks passing Dianchi Lake typically from January to March and from August to November in each year. Figure 9 shows the lake level time series of retracked surface heights above the EGM2008 geoid over Dianchi Lake from late 2010 to early 2019, derived from official ICE (in blue), ALES (in green) and MBP (in magenta) retrackers. The peaks of lake level fluctuations are ~4 m and ~2 m for retracked

surface heights by official ICE and ALES/MBP retrackers, respectively. A common feature is that the lake levels derived from three retrackers are low in August or September and high in March or November. When taking into account of no CryoSat-2 data from April to July and in December over Dianchi Lake, this feature is consistent with variations of the monthly mean lake level over Dianchi Lake derived using in situ gauge data in [25], where the mean lake level of Dianchi Lake was found to reach the lowest level in May and June, and the highest level from October to December.

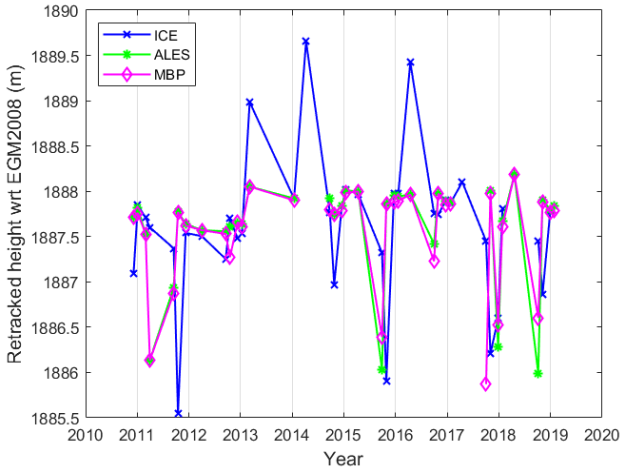

Figure 9. Lake level variations of Dianchi Lake from retrackers of ICE, ALES and MBP over the period of 2010–2019.

4.2.3. Validation

Although there are gauge stations around Dianchi Lake to collect measurements including the precipitation, evaporation and lake level [25], the in situ measurements of lake level are not available to the authors. Thus, we adopted the annual lake levels in [25,26] as the in situ truth of Dianchi Lake over in the period of 1988–2016 to validate our retracked lake level from this study. In order to be compatible with the in situ data, we generated the annual lake level using a median value of retracked surface heights of the year and computed its standard deviation (Figure 10 and Table 4). It can be seen from left graph in Figure 10 that the annually mean lake levels dropped to the lowest level (~1887.70 m) in 2012 and reached the highest (~1887.96 m) in 2015 and 2016 during the period of 2011–2019, while the annual in situ lake level had the highest value (~1887.40 m) in 2014 during the period of 1988–2016 [25,26].

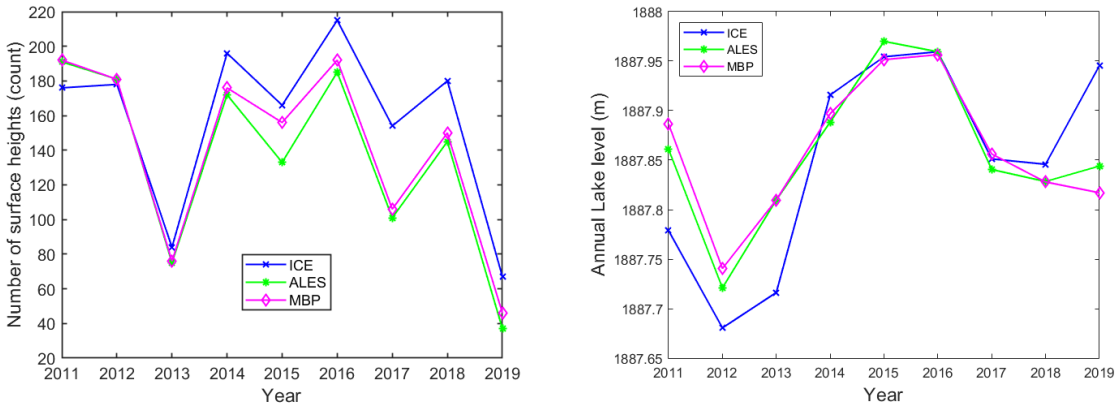

Figure 10. The annual lake level derived from retrackers of ICE, ALES and MBP over Dianchi Lake (**left**) and corresponding number of surface heights used to derive the annual level (**right**).

Table 4. Statistics of maximum, minimum and mean standard deviations of the annual lake level for Dianchi Lake (in m). The bold value indicates the smallest mean standard deviation.

Retracker	Min	Max	Mean
ICE	0.161	0.355	0.254
ALES	0.050	0.402	0.298
MBP	0.192	0.398	0.303

The right graph in Figure 10 shows the number of retracked heights that were used to determine the annual lake level of the year. It can be seen that the numbers of retracked lake levels are less than 80 in 2013 and 2019. The reason is that there were only two and one tracks of CryoSat-2 LRM data available in 2013 and early 2019, respectively. The ICE retracker retrieved the greatest number of lake levels every year compared to retrackers of ALES and MBP, which is expected because of its non-physical retracking characteristics. ALES and MBP retrackers have similar numbers of surface heights in each year, except for 2015 when the number of MBP retracked heights is more than that of ALES (~160 vs. ~135). Although ALES and MBP are applied to sub- and full-waveforms, respectively, they adopted the Brown model to retrieve the surface height [32,34]. Our previous research has shown that both retrackers have a similar performance, e.g., [32,33]. Therefore, it is reasonable that they achieved a similar number of retracked surface heights over Dianchi Lake.

Table 4 shows a statistical analysis of standard deviations of annual lake levels from different retrackers. The annual lake levels derived by the official ICE retracker achieves the smallest mean standard deviation of 0.254 m, suggesting that it is the most appropriate retracker for LRM waveforms over Dianchi Lake. ALES and MBP were originally designed for coastal waveforms with the clear water feature on the leading edge. They may not be capable of handling waveforms contaminated by land near the lake shoreline, in particular close to the north-west, east and south lake shorelines of Dianchi Lake. In addition, it is found that there are a certain number of specular or quasi-specular waveforms (not show) over Dianchi Lake, particularly over farming in the human-made littoral zone close to the lakeshore, where the surface roughness is relatively small. These waveforms cannot be properly processed by ALES and MBP retrackers, causing large errors in the lake surface height estimation.

There is an overlap period of six years (2011–2016) between time series of CryoSat-2 and in situ annual lake levels. Instead of directly comparing the annual lake levels of two types of time series, we again converted the annual lake levels to annual lake level anomalies. The median value of annual levels was found from eight years of lake levels between 2011–2018 for CryoSat-2 and 2009–2016 for the in situ data. The annual lake level anomalies are then computed by subtracting the median value from annual lake levels. Figure 11 compares the variations of annual lake level anomalies derived from in situ and CryoSat-2 LRM data by different retrackers. It can be visually seen that they agree well with each other over the period of 2011–2016.

We also computed the correlation coefficients and median absolute deviations between CryoSat-2 and in situ annual lake levels (2011–2016), as well as the trend of CryoSat-2 lake levels during the period of 2011–2019 (Table 5). The annual lake levels from ICE, ALES and MBP retrackers are all strongly correlated with those from in situ gauge data with correlation coefficients >0.89. The ICE retracked annual lake levels, among three retracked datasets, have the lowest noise level with the smallest median absolute deviation of 0.027 m. Since 2011, all lake level time series have in general shown an upward trend. The trend estimates computed from CryoSat-2 derived lake levels range from 28.8 to 36.7 mm/yr depending on the retracker during 2011–2019 (Table 5), while the trend of 25 mm/yr was estimated from in situ lake levels over the period of 1988–2015 in [25]. The difference between the trends from CryoSat-2 and in situ lake levels is most likely caused by different data periods (27-year in situ data vs. 9-year CryoSat-2 data). When taking into account the smallest mean standard deviation (0.254 m) of the lake level, the smallest median absolute

deviation (0.027 m) with respect to in situ data, and the highest correlation coefficient (0.96), ICE retracker is superior to ALES and MBP retrackers for CryoSat-2 LRM waveforms in Dianchi Lake. This again suggests that the official ICE retracked CryoSat-2 LRM data products can be directly used to monitor the water level fluctuations over Dianchi Lake. Although ALES and MBP have been proven to be efficient for retracking coastal waveforms, the results from this study suggest that the further modification of retracking procedure is necessary for applying both retrackers to CryoSat-2 LRM waveforms over inland lakes, which will be our future research.

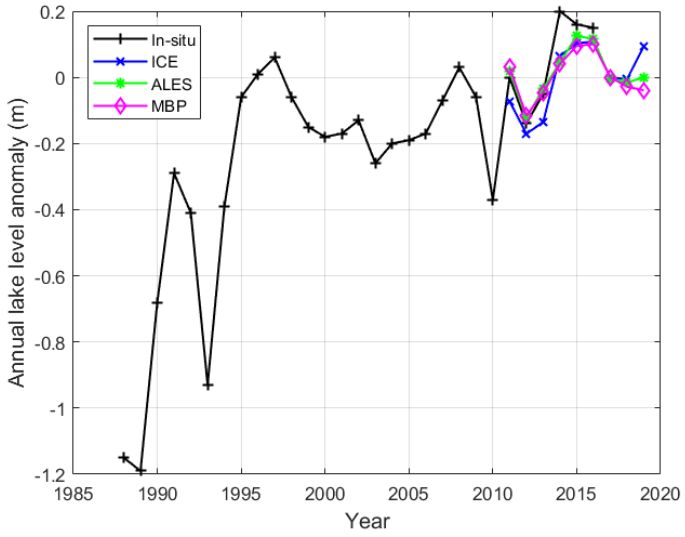

Figure 11. Validation of variations of annual lake level anomalies derived from CryoSat-2 LRM against those from in situ gauge data in Dianchi Lake from 2011 to 2016. Here, we adopted the annual lake levels in [25,26] as the in situ truth (in black) of Dianchi Lake over the period of 1988–2016.

Table 5. Estimates of trends of CryoSat-2 derived lake levels (2011–2019), correlation coefficients and median absolute deviation (MAD) between CryoSat-2 LRM and in situ annual lake levels (2011–2016) over Dianchi Lake.

Retracker	ICE	ALES	MBP
Trend (mm/yr)	30.9 ± 64.9	28.8 ± 64.9	36.7 ± 73.0
Correlation	0.96	0.90	0.89
MAD (m)	0.027	0.046	0.055

It is noted in Table 5 that the trend estimates are correspondent to the large uncertainties. This suggests that the trend is not linear within the nine years of observations. Although the results obtained are interesting to be shown, the accurate trend estimation for Dianchi Lake requires a long-term time series from CryoSat-2 LRM data.

5. Conclusions

In this paper, CryoSa-2 L2 LRM and L1B SARIn-mode data from 2011 to 2018 have been used to monitor water level variations of Dianchi Lake and two lakes in TP (i.e., Gemang Co and Zhangnai Co), respectively. In addition to official data estimated from ICE (for LRM) and WWMFW (for SARIn) retrackers, we have retrieved the water surface heights referred to the EGM2008 geoid through retracking CryoSat-2 20 Hz waveforms using different retrackers, including ALES and MBP (for LRM), as well as PPT, OCOG and APD-PPT (for SARIn). Of these retrackers, the APD-PPT is newly proposed in this study, which combines the adaptive peak detection method with the PPT. The lake level is determined via the median value and standard deviation computed from the outlier-free

and unbiased surface heights along each track. The time series of lake levels has been generated and its trend has been estimated for each lake over the study period.

Two TP lakes are relatively small with areas of 36 km^2 (Zhangnai Co) and 52 km^2 (Gemang Go) and passed by at the least two CryoSat-2 SARIn ground tracks in each repeat cycle. The along-track surface height profiles from different retrackers have shown a similar variation pattern. The trends of lake level time series are computed. The estimated trends in relation to different retrackers range from 51.1 to 61.0 mm/yr for Zhangnai Co, and from 51.3 to 76.9 mm/yr for Gemang Co, suggesting that both lake levels had a continuous rise during 2011–2018. When compared to other retrackers, the new APD-PPT retracker achieves the smallest mean standard deviations when creating the lake level from along-track surface heights, with 0.303 m (vs 0.344-0.433 m) for Gemang Co and 0.186 m (vs. 0.204–0.284 m) for Zhangnai Co. This indicates that APD-PPT is the most appropriate retracker for SARIn-mode waveforms over small lakes in TP, where waveforms are most likely polluted by surrounding land topography.

The lake level time series from CryoSat-2 over Zhangnai Co is validated against that from Jason-2 data during 2009–2015 by Hwang et al. [13]. The validation results show a strong correlation (>0.73) between two types of time series of lake levels. The trend estimates over Znahgnai Co have good agreement with the trend (59.9 mm/yr) computed from Jason-2 data during 2009–2015. The results suggest that lake level variations can be efficiently monitored through retracking CryoSat-2 SARIn-mode 20Hz waveforms over relatively small lakes.

For Dianchi Lake sampled by CryoSat-2 LRM measurements, two retrackers of ALES and MBP are used in addition to the official ICE retracker. The retracked surface heights are low in August or September and high in March or November in each year, being consistent with those derived from in situ data in [25]. The annual lake level from CryoSat-2 is also found to be strongly correlated (>0.89) with that from in situ data in [25]. The trend estimates computed from CryoSat-2 derived lake levels range from 28.8 to 36.7 mm/yr depending on the retracker during 2011–2019, which are slightly different from the trend of 25 mm/yr estimated from in situ lake levels over the period of 1988–2015 in [25]. It is also found that a long-term time series of lake levels (>9 years) is needed to estimate a robust linear trend for Dianchi Lake. When considering the standard deviation of annual lake levels, value of correlation coefficient between annual lake levels from CryoSat-2 LRM and in situ data, and median absolute deviation (i.e., data noise) with respect to in situ data, it is found that the official ICE retracker has the best performance over Dianchi Lake.

The challenge still remains in retracking CryoSat-2 LRM waveforms near lake shorelines, where the fitting algorithms used in ALES and MBP retrackers may fail to handle the contaminated and/or specular waveforms. It is necessary to further improve the retracker and hence the quality of retracked lake surface heights.

Of about 1400 lakes with the area >1 km^2 in TP plateau, only about a tenth of the lakes, mostly >100 km^2, has been thus far monitored using satellite altimetry measurements from the open literature. The CryoSat-2′s long and drifting 369-day orbit, as well as its small footprint (330 m) in the along-track direction, have made it possible to sample many TP lakes though it passes different parts of the lake in the same repeat cycle. In this regard, the methods of this study have the potential to be used for many small lakes that have not been measured by other altimetry missions in TP plateau.

Lake level fluctuations are naturally associated with climate variability. Total lake area in TP, in particular in the northwestern TP, has been found to continuously increase since 1976 due mainly to the global warming, e.g., [1,8,13,43]. In the case that the lake level variations can be determined in as many lakes as possible, we will be able to accurately detect the lake storage changes in TP and, thus, better understand how climate change influences the lake level evolutions.

Author Contributions: Conceptualization, X.D.; methodology, X.D. and F.P.; software, X.D. and F.P.; validation, X.D.; formal analysis, X.D. and F.P.; investigation, X.D.; data curation, R.-B.W. and Y.Y.; writing—original draft preparation, X.D.; writing—review and editing, all authors; visualization, X.D. and F.P.; project administration, R.-B.W., X.D.; funding acquisition, R.-B.W., X.D., and N.-M.M. All authors have read and agreed to the published version of the manuscript.

Funding: This research was partly funded by a research project by Yunnan Province, China, grant number YN2020018.

Acknowledgments: We thank European Space Agent for providing the CryoSat-2 data, Professor Cheinway Hwang and Professor Changqun Duan for providing Jason-2 and in situ annual lake level data, respectively, for validation in this study, and the Postdoc Xin Luo for providing the water mask of Dianchi Lake. The authors would like to thank Professor Mark Stewart for reviewing and proof reading the manuscript. We also thank the anonymous reviewers and the editor for their comments on this manuscript.

Conflicts of Interest: The authors declare no conflict of interest. The founding sponsors had no role in the design of the study; in the collection, analyses, or interpretation of data; in the writing of the manuscript; or in the decision to publish the results.

References

1. Zhang, G.; Chen, W.; Li, G.; Yang, W.; Yi, S.; Luo, W. Lake water and glacier mass gains in the northwestern Tibetan Plateau observed from multi-sensor remote sensing data: Implication of an enhanced hydrological cycle. *Remote Sens. Environ.* **2020**, *237*, 111554. [CrossRef]
2. Wang, L. Moving Towards Integrated Management of the Plateau Lakes in Yunnan Province, China. Available online: https://ilec.or.jp/ILBMTrainingMaterials/authors (accessed on 12 March 2021).
3. Kleinherenbrink, M.; Lindenbergh, R.; Ditmar, P. Monitoring of lake level changes on the Tibetan Plateau and Tian Shan by retracking Cryosat SARIn waveforms. *J. Hydrol.* **2015**, *521*, 119–131. [CrossRef]
4. Jiang, L.; Schneider, R.; Andersen, O.B.; Bauer-Gottwein, P. CryoSat-2 Altimetry Applications over Rivers and Lakes. *Water* **2017**, *9*, 211. [CrossRef]
5. Crétaux, J.-F.; Calmant, S.; Romanovski, V.; Shabunin, A.; Lyard, F.; Bergé-Nguyen, M.; Cazenave, A.; Hernandez, F.; Perosanz, F. An absolute calibration site for radar altimeters in the continental domain: Lake Issykkul in Central Asia. *J. Geod.* **2008**, *83*, 723–735. [CrossRef]
6. Crétaux, J.-F.; Abarca-Del-Río, R.; Bergé-Nguyen, M.; Arsen, A.; Drolon, V.; Clos, G.; Maisongrande, P. Lake Volume Monitoring from Space. *Surv. Geophys.* **2016**, *37*, 269–305. [CrossRef]
7. Hwang, C.; Chu, Y.; Huang, Z.; Chao, N. Robust, Long-term Lake Level Change from Multiple Satellite Altimeters in Tibet: Observing the Rapid Rise of Ngangzi Co over a New Wetland. *Remote Sens.* **2019**, *11*, 558. [CrossRef]
8. Hwang, C.; Cheng, Y.-S.; Yang, W.-H.; Zhang, G.; Huang, Y.-R.; Shen, W.-B.; Pan, Y. Lake level changes in the Tibetan Plateau from Cryosat-2, SARAL, ICESat, and Jason-2 altimeters. *Terr. Atmos. Ocean. Sci.* **2019**, *30*, 33–50. [CrossRef]
9. Jiang, L.; Andersen, O.B.; Nielsen, K.; Zhang, G.; Bauer-Gottwein, P. Influence of local geoid variation on water surface elevation estimates derived from multi-mission altimetry for Lake Namco. *Remote Sens. Environ.* **2019**, *221*, 65–79. [CrossRef]
10. Kao, H.-C.; Kuo, C.-Y.; Tseng, K.-H.; Shum, C.; Tseng, T.-P.; Jia, Y.-Y.; Yang, T.-Y.; Ali, T.A.; Yi, Y.; Hussain, D. Assessment of Cryosat-2 and SARAL/AltiKa altimetry for measuring inland water and coastal sea level variations: A case study on Tibetan Plateau lake and Taiwan Coast. *Mar. Geod.* **2019**, *42*, 327–343. [CrossRef]
11. Li, X.; Long, D.; Huang, Q.; Han, P.; Zhao, F.; Wada, Y. High-temporal-resolution water level and storage change data sets for lakes on the Tibetan Plateau during 2000–2017 using multiple altimetric missions and Landsat-derived lake shoreline positions. *Earth Syst. Sci. Data* **2019**, *11*, 1603–1627. [CrossRef]
12. Song, C.; Ye, Q.; Cheng, X. Shifts in water-level variation of Namco in the central Tibetan Plateau from ICESat and CryoSat-2 altimetry and station observations. *Sci. Bull.* **2015**, *60*, 1287–1297. [CrossRef]
13. Hwang, C.; Cheng, Y.-S.; Han, J.; Kao, R.; Huang, C.-Y.; Wei, S.-H. Multi-Decadal Monitoring of Lake Level Changes in the Qinghai-Tibet Plateau by the TOPEX/Poseidon-Family Altimeters: Climate Implication. *Remote Sens.* **2016**, *8*, 446. [CrossRef]
14. Bouzinac, C. CryoSat-2 Product Handbook. 2014. Available online: https://earth.esa.int/documents/10174/125272/CryoSat_Product_Handbook (accessed on 12 March 2020).
15. Wingham, D.; Francis, C.; Baker, S.; Bouzinac, C.; Brockley, D.; Cullen, R.; de Chateau-Thierry, P.; Laxon, S.; Mallow, U.; Mavrocordatos, C.; et al. CryoSat: A mission to determine the fluctuations in Earth's land and marine ice fields. *Adv. Space Res.* **2006**, *37*, 841–871. [CrossRef]
16. Villadsen, H.; Deng, X.; Andersen, O.B.; Stenseng, L.; Nielsen, K.; Knudsen, P. Improved inland water levels from SAR altimetry using novel empirical and physical retrackers. *J. Hydrol.* **2016**, *537*, 234–247. [CrossRef]
17. Jain, M.; Andersen, O.B.; Dall, J.; Stenseng, L. Sea surface height determination in the Arctic using Cryosat-2 SAR data from primary peak empirical retrackers. *Adv. Space Res.* **2015**, *55*, 40–50. [CrossRef]

18. Villadsen, H.; Andersen, O.B.; Stenseng, L.; Nielsen, K.; Knudsen, P. CryoSat-2 altimetry for river level monitoring—Evaluation in the Ganges–Brahmaputra River basin. *Remote Sens. Environ.* **2015**, *168*, 80–89. [CrossRef]
19. Kleinherenbrink, M.; Ditmar, P.; Lindenbergh, R. Retracking Cryosat data in the SARIn mode and robust lake level extraction. *Remote Sens. Environ.* **2014**, *152*, 38–50. [CrossRef]
20. Roohi, S.; Sneeuw, N.; Benveniste, J.; Dinardo, S.; Issawy, E.; Zhang, G. Evaluation of CryoSat-2 water level derived from different retracking scenarios over selected inland water bodies. *Adv. Space Res.* **2019**. [CrossRef]
21. Wingham, D.J.; Rapley, C.G.; Griffiths, H. New Techniques in Satellite Tracking Systems. In Proceedings of the IGARSS' 88 Symposium, Zurich, Switzerland, 8–11 September 1986; pp. 1339–1344.
22. Davis, C. Growth of the Greenland ice sheet: A performance assessment of altimeter retracking algorithms. *IEEE Trans. Geosci. Remote Sens.* **1995**, *33*, 1108–1116. [CrossRef]
23. Cheng, H.; Yang, J.; Lu, Z.; Zhang, L. The flow field simulation on Dianchi Lake. *Procedia Eng.* **2012**, *31*, 696–702. [CrossRef]
24. Hou, P.; Luo, Y.; Yang, K.; Shang, C.; Zhou, X. Changing Characteristics of Chlorophyll a in the Context of Internal and External Factors: A Case Study of Dianchi Lake in China. *Sustainability* **2019**, *11*, 7242. [CrossRef]
25. Kediao, H.; Wei, G.; Changqun, D.; Yuangao, Z.; Ying, P.; Chang'E, L.; Wei, Z.; Guiying, Y. Water level variation and its driving factors in Lake Dianchi, Fuxian and Yangzong during 1988. *J. Lake Sci.* **2019**, *31*, 1379–1390. [CrossRef]
26. Wen, D.; Jin, C.; Shixiang, G.; Gang, C.; Jinming, C.; Mi, Z. Hydrological Variability of Water Level of Dianchi Lake and Its Application. *IOP Conf. Series Mater. Sci. Eng.* **2020**, *780*, 062048. [CrossRef]
27. Yang, K.; Yu, Z.; Luo, Y.; Yang, Y.; Zhao, L.; Zhou, X. Spatial and temporal variations in the relationship between lake water surface temperatures and water quality—A case study of Dianchi Lake. *Sci. Total. Environ.* **2018**, *624*, 859–871. [CrossRef]
28. Wang, X.; Pang, G.; Yang, M. Precipitation over the Tibetan Plateau during recent decades: A review based on observations and simulations. *Int. J. Clim.* **2018**, *38*, 1116–1131. [CrossRef]
29. Abulaitijiang, A.; Andersen, O.B.; Stenseng, L. Coastal sea level from inland CryoSat-2 interferometric SAR altimetry. *Geophys. Res. Lett.* **2015**, *42*, 1841–1847. [CrossRef]
30. Hayne, G. Radar altimeter mean return waveforms from near-normal-incidence ocean surface scattering. *IRE Trans. Antennas Propag.* **1980**, *28*, 687–692. [CrossRef]
31. Wingham, D.J.; Wallis, D.W. The Rough Surface Impulse Response of a Pulse-Limited Altimeter with an Elliptical Antenna Pattern. *IEEE Antennas Wirel. Propag. Lett.* **2010**, *9*, 232–235. [CrossRef]
32. Peng, F.; Deng, X. A New Retracking Technique for Brown Peaky Altimetric Waveforms. *Mar. Geodesy* **2017**, *41*, 99–125. [CrossRef]
33. Peng, F.; Deng, X. Validation of Sentinel-3A SAR mode sea level anomalies around the Australian coastal region. *Remote Sens. Environ.* **2020**, *237*, 111548. [CrossRef]
34. Passaro, M.; Cipollini, P.; Vignudelli, S.; Quartly, G.D.; Snaith, H.M. ALES: A multi-mission adaptive subwaveform retracker for coastal and open ocean altimetry. *Remote Sens. Environ.* **2014**, *145*, 173–189. [CrossRef]
35. Brown, G. The average impulse response of a rough surface and its applications. *IRE Trans. Antennas Propag.* **1977**, *25*, 67–74. [CrossRef]
36. Peng, F.; Deng, X. Improving precision of high-rate altimeter sea level anomalies by removing the sea state bias and intra-1-Hz covariant error. *Remote Sens. Environ.* **2020**, *251*, 112081. [CrossRef]
37. Peng, F.; Deng, X. Validation of Wind Speeds from Brown-Peaky Retracker in the Gulf of Mexico and East Coast of North America. *IEEE Trans. Geosci. Remote Sens.* **2020**, *58*, 5793–5803. [CrossRef]
38. Pavlis, N.K.; Holmes, S.A.; Kenyon, S.C.; Factor, J.K. The development and evaluation of the Earth Gravitational Model 2008 (EGM2008). *J. Geophys. Res. Space Phys.* **2012**, *117*, 117. [CrossRef]
39. Rosner, B. Percentage Points for a Generalized ESD Many-Outlier Procedure. *Technometrics* **1983**, *25*, 165–172. [CrossRef]
40. Deng, X.; Featherstone, W.E. A coastal retracking system for satellite radar altimeter waveforms: Application to ERS-2 around Australia. *J. Geophys. Res. Space Phys.* **2006**, *111*, 111. [CrossRef]
41. Kropáček, J.; Maussion, F.; Chen, F.; Hoerz, S.; Hochschild, V. Analysis of ice phenology of lakes on the Tibetan Plateau from MODIS data. *Cryosphere* **2013**, *7*, 287–301. [CrossRef]
42. Lei, Y.; Zhu, Y.; Wang, B.; Yao, T.; Yang, K.; Zhang, X.; Zhai, J.; Ma, N. Extreme Lake Level Changes on the Tibetan Plateau Associated With the 2015/2016 El Niño. *Geophys. Res. Lett.* **2019**, *46*, 5889–5898. [CrossRef]
43. Yao, F.; Wang, J.; Yang, K.; Wang, C.; A Walter, B.; Crétaux, J.-F. Lake storage variation on the endorheic Tibetan Plateau and its attribution to climate change since the new millennium. *Environ. Res. Lett.* **2018**, *13*, 064011. [CrossRef]